The Cryosphere
Discussions

Open Access

EGU

Mechanisms influencing seasonal-to-interannual prediction skill of sea ice extent in the Arctic Ocean in MIROC

Jun Ono[1], Hiroaki Tatebe[1], Yoshiki Komuro[1], Masato I. Nodzu[2], Masayoshi Ishii[3]

[1] Japan Agency for Marine-Earth Science and Technology, Yokohama, 236-0001, Japan
5   [2] Tokyo Metropolitan University, Hachioji, 192-0397, Japan
[3] Meteorological Research Institute, Japan Meteorological Agency, Tsukuba, 305-0052, Japan

Correspondence to: Jun Ono (jun.ono@jamstec.go.jp)

Abstract. To assess the skill of predictions of the seasonal-to-interannual detrended sea ice extent in the Arctic Ocean (SIE$_{AO}$) and to clarify the underlying physical processes, we conducted ensemble hindcasts, started on January 1st, April 1st,
10   July 1st, and October 1st for each year from 1980 to 2011, for lead times of up three years, using the Model for Interdisciplinary Research on Climate (MIROC) version 5 initialized with the observed atmosphere and ocean anomalies and sea ice concentration. Significant skill is found for the winter months: the December SIE$_{AO}$ can be predicted up to 1 year ahead. This skill is attributed to the subsurface ocean heat content originating in the North Atlantic. The subsurface water flows into the Barents Sea from spring to fall and emerges at the surface in winter by vertical mixing, and eventually affects
15   the sea ice variability there. Meanwhile, the September SIE$_{AO}$ predictions are skillful for lead times of up to 3 months, due to the persistence of sea ice in the Beaufort, Chukchi, and East Siberian Seas initialized in July, as suggested by previous studies.

1 Introduction

The Arctic has warmed more than twice as much as the global average (e.g., Bekryaev et al., 2010; Cohen et al.,
20   2014), called Arctic amplification. Sea ice reduction under climate change is one of the main processes contributing to Arctic amplification (e.g., Pithan and Mauritsen, 2014). Arctic summer sea ice extent has declined at about 14 % per decade (National Snow and Ice Data Center, 2016, http://nsidc.org/arcticseaicenews/). In September 2012, sea ice extent reached its minimum since satellite observations began in the late 1970s. An even more serious problem is the decline in Arctic sea ice thickness (Kwok et al., 2009), which has decreased by around 65 % from 1975 to 2012 (Lindsay and Schweiger, 2015).

25   In contrast to the rapid warming in the Arctic, severely cold winters have occurred more frequently at midlatitudes. Although the exact cause is still being debated (e.g., Barnes and Screen, 2015), Mori et al. (2014) have shown, using ensemble experiments with an atmospheric general circulation model, that the more frequent cold winters at midlatitudes can be partly explained by the sea ice decrease in the Barents and Kara Seas. Therefore, further investigation of the mechanisms driving Arctic sea ice variability is of great importance for more accurate predictions of climate change, not only in the
30   Arctic but also for the midlatitudes.

A previous study based on two- or five-year perfect-model experiments from January 1st and September 1st has shown that the potential predictability for sea ice extent is continuously one to two years, primarily because of the persistence of ice thickness anomalies from summer to summer and the persistence of sea surface temperature anomalies from the melt to growth seasons (Blanchard-Wrigglesworth et al., 2011a; Guemas et al., 2014). These features are also found in the results of experiments comparing multiple climate models (Day et al., 2014b; Tietsche et al., 2014). The observed Arctic sea ice extent based on ensemble hindcasts can be predicted up to 2–7 and 5–11 months ahead for summer and winter, respectively (e.g., Chevallier et al., 2013; Sigmond et al., 2013; Wang et al., 2013; Msadek et al., 2014; Peterson et al., 2015; Guemas et al., 2016; Sigmond et al., 2016). In these ensemble hindcasts, it is found that the ice thickness and the surface or subsurface water temperatures are closely related to the prediction skill, as suggested by idealized or perfect-model experiments with climate models (e.g., Blanchard-Wrigglesworth et al., 2011b; Chevallier and Salas-Mélia, 2012; Day et al., 2014a).

Until very recently, the mechanisms by which the above variables contribute to the prediction skill had not been quantified. Bushuk et al. (2017) examined the physical mechanisms underlying the prediction skill of regional sea ice extent and showed for the first time the importance of the initializations of ocean subsurface and sea ice thickness in their dynamical prediction system.

Motivated by the above studies, we first conduct initialized ensemble hindcasts using a climate model to assess the predictability of seasonal-to-interannual sea ice extent in the Arctic Ocean and further investigate sources for prediction skill and clarify the physical processes linking the prediction skill to its sources. In particular, the present study reveals that subsurface ocean heat content originating from the North Atlantic contributes to the predictability of winter sea ice through advection and vertical mixing processes, which is somewhat different from the reemergence process of the local subsurface ocean temperature suggested by Bushuk et al. (2017).

2 Experimental Designs

The climate model used here is a low-resolution version of the Model for Interdisciplinary Research on Climate, version 5 (MIROC5) (Watanabe et al., 2010), which contributed to the fifth phase of the Coupled Model Intercomparison Project and the Intergovernmental Panel on Climate Change Fifth Assessment Report (IPCC AR5, 2013). The atmospheric component has a horizontal resolution of T42 spectral truncation (approximately 2.8°) and comprises 40 vertical layers up to 3 hPa. The oceanic component has horizontal resolutions of 1.4° in longitude and 0.5–1.4° in latitude, and comprises 50 vertical layers. The sea ice component of MIROC5 contains one-layer thermodynamics (Bitz and Lipscomb, 1999), elastic-viscous-plastic rheology (Hunke and Dukowicz, 1997), and the subgrid ice thickness distribution (Bitz et al., 2001) with five categories: the detailed structure has been described in Komuro et al. (2012).

To initialize MIROC5, we adopted anomaly assimilation for the atmosphere and ocean and full-field assimilation for sea ice. Anomalies were calculated as the deviations from the climatology defined by the 1961–2000 period. The observed 6-hourly air temperature and wind vectors from the 55-year Japanese Reanalysis (JRA-55) dataset (Kobayashi et

al., 2015) were linearly interpolated to the atmospheric model's grid. The observed monthly temperature, salinity, and sea ice concentration (SIC) from the gridded monthly objective analysis produced by Ishii et al. (2006) and Ishii and Kimoto (2009) were linearly interpolated to obtain the daily values, and the same grid as the ocean model. In the assimilation runs, the atmospheric anomalies were assimilated into MIROC5 below 100 hPa at 6-hourly intervals and the oceanic anomalies above

5 3000 m depth at one-day intervals except in sea ice regions, using a modified incremental analysis update scheme (Tatebe et al., 2012). Meanwhile, SIC was assimilated at one-day intervals following Lindsay and Zhang (2006) and Stark et al. (2008). These assimilations were conducted over the period 1975–2011 with eight ensemble members produced by perturbing the sea surface temperature based on the observational errors. The atmospheric and oceanic initial states were obtained from a non-initialized twentieth-century run with historical natural and anthropogenic forcings.

10 On the basis of the assimilation runs, the hindcast experiments were integrated for 3 years from January 1st, 2 years and 9 months from April 1st, 2 years and 6 months from July 1st and 2 years and 3 months from October 1st for each year from 1980 to 2011. The initial states of the atmosphere and ocean were obtained from the corresponding assimilation runs. In addition, a control run with MIROC version 5.2, which is a minor update of MIROC5, was used to interpret the physical processes contributing to the prediction skill in the hindcasts. This simulation was run with external forcings fixed at the year

15 2000 levels under a multi-model inter-comparison project (Day et al., 2016).

In Sect. 3 and Sect. 4, we analyze the detrended monthly anomalies to extract the internal variations with seasonal-to-interannual timescales. Here, the detrended components were calculated by subtracting monthly linear trends during 1980–2009 from the original monthly data, and anomalies are defined as deviations from the climatology from 1980–2009. Moreover, climate drifts in the hindcasts are removed according to the INTERNATIONAL CLIVAR PROJECT OFFICE

20 (ICPO, 2011). As mentioned in Sect. 1, sea ice reduction in the Arctic Ocean, especially in the Barents and Kara Seas, could lead to extreme weather at midlatitudes, which may be related to the warming of the Arctic Ocean interior (e.g., Polyakov et al., 2012). To clearly interpret the physical mechanisms influencing sea ice extent in the Arctic Ocean (hereafter SIE_{AO}), SIE_{AO} is defined from the cumulative area for all grid cells north of 65° N with SIC greater than 15 %. Note that Hudson Bay and Baffin Bay are excluded. For comparison, the results for the detrended sea ice extent anomaly in the Northern

25 Hemisphere are shown in the supporting information.

3 Predictability of Arctic Sea Ice Extent

We first examine the potential predictability of SIE_{AO} (Fig. 1), based on the lagged auto-correlation coefficients, which is called the persistence forecast. The lagged correlations with the observations (Ishii et al. (2006) and Ishii and Kimoto (2009)) decrease within the first few months for all of the start months, and those originating between January and

30 June subsequently rise again in the winter (November through March). In addition, the correlation coefficients are higher than those shown in Day et al. (2014b), for example, at a lead time of one month for May. This may be due to differences in the observations, temporal periods, and areas used for calculating the sea ice extent (Fig. S1). Significant skill in the control

run is obtained for greater lead times than in the observations, which is consistent with previous studies (e.g., Blanchard-Wrigglesworth et al., 2011b; Day et al., 2014b).

We next evaluate the SIE_{AO} prediction skill (Figs. 2a and 2b), with the anomaly correlation coefficient (ACC) and the root-mean-square error (RMSE) between the detrended observations and the hindcasts (e.g., Wang et al., 2013). In the
5   hindcasts started from July 1st, the ACC for September is statistically significant and exceeds that of the persistence forecast, suggesting that September SIE_{AO} can be dynamically predicted from the previous July. Although the significance of the ACC is borderline, the results suggest September SIE_{AO} is potentially predictable from April 1st, which is consistent with the results of Peterson et al. (2015). The ACC is also significant for the winter SIE_{AO}, in particular for December, except for the hindcasts started from April 1st, indicating the potential use of dynamical forecasts up to 1 year ahead. The RMSE for all
10 hindcasts increases throughout the melting and early freezing seasons (July–October), before decreasing in November–June. These seasonal changes in the RMSE are consistent with past studies (e.g., Tietsche et al., 2014). The time series of September SIE_{AO} shows that both the assimilation and hindcasts capture the observed interannual variability, although the model underestimates the variability in the mid- to late 1980s and in the extreme year 2007 (Fig. 2c). The observed SIE_{AO} in December is contained within the ensemble spread, excluding the mid-1980s (Fig. 2d). We also show the same figure as Fig.
15 2 in Fig. S2, except that the detrended sea ice extent anomaly is calculated in the Northern Hemisphere. Although the RMSE in winter is high (Fig. S2b) compared to Fig. 2b, there are no significant differences.

4 Possible Mechanisms for Prediction Skill

Focusing on both the hindcasts started from January 1st, in which the December SIE_{AO} has high skill even at the longest lead-time, and those started from July 1st, in which only the September SIE_{AO} is significant, we examine
20 mechanisms for the prediction skill. Figure 3 shows the lagged cross-correlations between the SIE_{AO} and the sea ice volume in the Arctic Ocean (SIV_{AO}) and those between SIE_{AO} and ocean heat content in the Arctic Ocean (OHC_{AO}) for the control run and the hindcasts started from January and July. Here, the SIV_{AO} is defined as the sum of the grid cell volumes obtained by multiplying the sea ice thickness (SIT) by the SIC for grid cells with SIC greater than 15 % and the OHC_{AO} is the vertically integrated temperature multiplied by the density and specific heat capacity of seawater from the mixed layer depth
25 (MLD) to a depth of 200 m, in the area north of 65° N. The MLD is defined as the depth at which the potential density differs from that of the surface by 0.01 kg m^{-3}.

The SIV_{AO} has stronger positive correlations with the SIE_{AO} in summer than in winter (Figs. 3a–c), which is consistent with Chevallier and Salas-Mélia (2012), while the OHC_{AO} has more persistent negative correlations with the SIE_{AO} in winter than in summer (Figs. 3d–f). In the hindcasts started from January 1st, the December SIE_{AO} is significantly
30 correlated with the OHC_{AO} from May to December. In the hindcasts started from July 1st, the SIE_{AO} in September is significantly correlated with the SIV_{AO} in July, but not with the OHC_{AO}. Thus, sources for the prediction skill of the December and September SIE_{AO} are suggested to be the subsurface OHC_{AO} after May through December and the sea ice states in July, respectively. For the sea ice extent anomaly calculated in the Northern Hemisphere (Fig. S3), the patterns of

lagged correlation coefficients are broadly similar to those in Fig. 3, but the correlations in the control are stronger and those in the hindcasts are weaker. One reason might be the contribution of sea ice variability south of 65° N.

We next clarify the physical processes linking the prediction skill to sources of that skill. Figure 4 shows the SIC, SIT, and OHC north of 60° N regressed on the December SIE_{AO}. We also show the same figure as Fig. 4 except that the detrended sea ice extent anomaly is calculated in the Northern Hemisphere (Fig. S4). The most significant signals for both SIC and SIT are found in the Barents Sea (BS) of the Arctic Ocean (Figs. 4a and 4b). It is well known that winter sea ice variability in the BS dominates that in the Arctic Ocean (e.g., Smedsrud et al., 2013), which is consistent with our results. At a lag of 9 months (Fig. 4c), negative correlation and regression coefficients for the OHC are found off the western coast of the Scandinavian Peninsula. Their signals become stronger along the Norwegian Atlantic Current pathway and in the western part of the BS at a lag of 6 months (Fig. 4d), and further extend across the entire BS at a lag of 3 months (Fig. 4e). Eventually, the signals reach the eastern part of the BS at a lag of zero (Fig. 4f), and disappear in the western part of the BS where the positive SIC regression coefficient is highly significant (Fig. 4a) and the OHC from the surface to the MLD shows significant negative correlation and regression patterns (Fig. S5). These results are indirect evidence of the subsurface OHC emergence to the surface by vertical mixing in winter.

The above features are also found in the control run (Fig. S6), suggesting that the advection processes of the OHC in the hindcasts are not due to processes distorted by the influence of initialization or climate drift in MIROC5. Hence, the OHC anomalies initialized in the North Atlantic flow into the BS through advection, subsequently emerge at the surface due to vertical mixing in winter, and affect the December sea ice distribution in the BS and eventually in the Arctic Ocean. This is one of the reasons why the hindcasts started from January 1st have significant skill for the December SIE_{AO}. As suggested by Bushunk et al. (2017), our results also suggest that the initialization of subsurface ocean temperature contributes to the skillful prediction of the winter sea ice extent in the BS. However, the underlying mechanisms are partly different in that the advection process from the North Atlantic is important in our results, which is consistent with results based on statistical methods using reanalysis data (e.g., Nakanowatari et al., 2014).

For September, the persistence of sea ice states initialized in July persists until September in the Beaufort, Chukchi, and East Siberian Seas (Fig. S7), which is consistent with Bushuk et al. (2017). Consequently, this persistence contributes to the prediction skill of the September SIE_{AO}. In contrast, possible mechanisms or sources cannot be detected in the hindcasts started from April 1st (Fig. S8), at least from the lagged correlation and regression analyses, although the September SIE_{AO} is weakly correlated with the SIV_{AO} and the OHC_{AO}.

5 Concluding Remarks

We investigated the predictability of the detrended SIE_{AO} anomaly and its sources based on an ensemble of hindcasts using an initialized climate model, MIROC5, and further identified physical processes related to the prediction skill. Prediction skill for Arctic winter SIE_{AO} is significantly higher than the persistence forecast, especially for December, indicating the possibility for dynamical forecasting one year ahead. The December SIE_{AO} is significantly correlated with the

December SIC and SIT in the BS where the subsurface OHC anomalies are advected from the North Atlantic, and subsequently emerge at the surface in winter, and contribute to the sea ice variability there. Our results suggest that sources of the December SIE_{AO} prediction skill exist in the North Atlantic and thus initialization of the subsurface water there leads to better prediction of the SIE_{AO} in December. Numerical experiments to confirm whether the subsurface OHC anomalies

5   originating from the North Atlantic control the December sea ice extent in the BS and eventually in the Arctic Ocean will be explored in future work.

Significant skill for the September SIE_{AO} is seen only up to 3 months ahead. Nevertheless, we note that the forecast skill of summer SIE_{AO} is not necessarily low, because the hindcasts initialized in January and April have significant skills for SIE_{AO} in August and September. Improvement in the prediction skill for summer SIE_{AO} is dependent upon refinement of the

10   initial state of the SIT. In fact, higher lagged correlations between the summer SIE_{AO} and the SIV_{AO} suggest the initialization of the SIT is important, which is consistent with previous results by Day et al. (2014a) and Bushuk et al. (2017).

In recent years, the rapid reduction in Arctic sea ice has enabled ships to navigate the Northern Sea Route (e.g., Stephenson et al., 2014). Under such maritime activities in the Arctic Ocean, forecasts of the local sea ice distribution rather than the total sea ice extent become of greater interest for marine users. Recent studies have reported the forecast skills of the

15   retreat and advance dates of the sea ice distribution based on statistical methods (e.g., Stroeve et al., 2016; Wang et al., 2016) as well as a dynamical forecast system (Sigmond et al., 2016; Bushuk et al., 2017). In the present study, our hindcasts could not reproduce precise sea-ice edges from summer to fall. For example, the predicted sea ice distributions in September 2007 are overestimated in the Russian region of the Arctic Ocean. This is because the surface winds, which are thought to be the major driving force of sea ice motion in September 2007, are not adequately predicted. Other reasons might be the lower

20   resolution of the ocean model or bias in the climatology. Further improvements in the predictability of sea ice, including its spatial pattern, will be provided by climate models with higher resolution, reduced model drift and bias, and improved initialization techniques.

Data availability. The data for this paper can be accessed via the authors for research purposes.

25

Competing interests. The authors declare that they have no conflict of interest.

References

"Arctic Sea Ice News & Analysis". National Snow and Ice Data Center. Accessed 7 September 2016.

Barnes, E. A. and Screen, J. A.: The impact of Arctic warming on the midlatitudes jet-stream: Can it? Has it? Will it?,
5   WIREs Clim Change 2015, 6:277-286, doi:10.1002/wcc.337, 2015.

Bekryaev, R. V., Polyakov, I. V., and Alexeev, V. A.: Role of polar amplification in long-term surface air temperature
variations and modern Arctic warming, J. Clim., 23, 3888-3906, doi:10.1175/2010JCLI3297.1, 2010.

10   Bitz, C. M. and Lipscomb, W. H.: An energy-conserving thermodynamic model of sea ice, J. Geophys. Res., 104, 15669-
15677, 1999.

Bitz, C. M., Holland, M. M., Weaver, A. J., and Eby, M.: Simulating the ice-thickness distribution in a coupled climate
model, J. Geophys. Res., 106, 2441-2463, 2001.

15

Blanchard-Wrigglesworth, E., Bitz, C. M., and Holland, M. M.: Influence of initial conditions and climate forcing on
predicting Arctic sea ice, Geophys. Res. Lett., 38, L18503, doi:10.1029/2011GL048807, 2011a.

Blanchard-Wrigglesworth, E., Armour, K. C., Bitz, C. M., and DeWeaver, E.: Persistence and inherent predictability of
20   Arctic sea ice in a GCM ensemble and observations, J. Clim., 24, 231-250, doi:10.1175/2010JCLI3775.1, 2011b.

Bushuk, M., Msadek, R., Winton, M., Vecchi, G. A., Gudgel, R., Rosati, A., and Yang, X.: Skillful regional prediction of
Arctic sea ice on seasonal timescales, Geophys. Res. Lett., 44, doi:10.1002/2017GL073155, 2017.

25   Chevallier, M. and Salas-Mélia, D.: The role of sea ice thickness distribution in the Arctic sea ice potential predictability: A
diagnostic approach with a coupled GCM, J. Clim., 25, 3025-3038, doi:10.1175/JCLI-D-11-00209.1, 2012.

Chevallier, M., Salas-Mélia, D., Voldoire, A., and Déqué, M.: Seasonal forecasts of the Pan-Arctic sea ice extent using a
GCM-based seasonal prediction system, J. Clim., 26, 6092-6104, doi:10.1175/JCLI-D-12-00612.1, 2013.

30

Cohen, J., Screen, J. A., Furtado, J. C., Barlow, M., Whittleston, D., Coumou, D., Franics, J., Dethloff, K., Entekhabi, D.,
Overland, J., and Jones, J.: Recent Arctic amplification and extreme mid-latitude weather, Nat. Geosci., 7, 627-637,
doi:10.1038/NGEO2234, 2014.

Day, J. J., Hawkins, E., and Tietsche, S.: Will Arctic sea ice thickness initialization improve seasonal forecast skill?, Geophys. Res. Lett., 41, 7566-7575, doi:10.1002/2014GL061694, 2014a.

5   Day, J. J., Tietsche, S., and Hawkins, E.: Pan-Arctic and regional sea ice predictability: Initialization month dependence, J. Clim., 27, 4371-4390, doi:10.1175/JCLI-D-13-00614.1, 2014b.

Day, J. J., Tietsche, S., Collins, M., Goessling, H. F., Guemas, V., Guillory, A., Hurlin, W. J., Ishii, M., Keeley, S. P. E., Matei, D., Msadek, R., Sigmond, M., Tatebe, H., and Hawkins, E.: The Arctic predictability and prediction on seasonal-to-
10 interannual timescales (APPOSITE) data set version 1, Geosci. Model Dev., 9, 2255-2270, doi:10.5194/gmd-9-2255-2016, 2016.

Guemas, V., Blanchard-Wrigglesworth, E., Chevallier, M., Day, J. J., Déqué, M., Doblas-Reyes, F. J., Fuckar, N. S., Germe, A., Hawkins, E., Keeley, S., Koenigk, T., Salas y Mélia, D., and Tietsche, S.: A review on Arctic sea-ice predictability and
15 prediction on seasonal to decadal time-scales, Q. J. R. Meteorol. Soc., doi:10.1002/qj.2401, 2014.

Guemas, V., Chevallier, M., Déqué, M., Bellprat, O., and Doblas-Reyes, F.: Impact of sea ice initialization on sea ice and atmosphere prediction skill on seasonal timescales, Geophys. Res. Lett., 43, 3889-3896, doi:10.1002/2015GL066626, 2016.

20 Hunke, E. C. and Dukowicz, J. K.: An elastic-viscous-plastic model for sea ice dynamics, J. Phys. Oceanogr., 27, 1849-1867, 1997.

INTERNATIONAL CLIVAR PROJECT OFFICE: Decadal and bias correction for decadal climate predictions, International CLIVAR Project Office, CLIVAR Publication Series No. 150 (not peer reviewed), 2011.
25

Ishii, M. and Kimoto, M.: Reevaluation of historical ocean heat content variations with time-varying XBT and MBT depth bias corrections, J. Oceanogr., 65, 287-299, doi:10.1007/s10872-009-0027-7, 2009.

Ishii, M., Kimoto, M., Sakamoto, K., and Iwasaki, S. I.: Steric sea level changes estimated from historical ocean subsurface
30 temperature and salinity analyses, J. Oceanogr., 62, 155-170, doi:10.1007/s10872-006-0041-y, 2006.

Kobayashi, S., Ota, Y., Harada, Y., Ebita, A., Moriya, M., Onoda, H., Onogi, K., Kamahori, H., Kobayashi, C., Endo, H., Miyaoka, K., and Takahashi, K.: The JRA-55 Reanalysis: General specifications and basic characteristics, J. Meteorol. Soc. Jpn., 93, 5-48, doi:10.2151/jmsj.2015-001, 2015.

Komuro, Y., Suzuki, T., Sakamoto, T. T., Hasumi, H., Ishii, M., Watanabe, M., Nozawa, T., Yokohata, T., Nishimura, T., Ogochi, K., Emori, S., and Kimoto, M.: Sea-ice in twentieth-century simulations by new MIROC coupled models: A comparison between models with high resolution and with ice thickness distribution, J. Meteorol. Soc. Jpn., 90A, 213–232, doi:10.2151/jmsj.2012-A11, 2012.

Kwok, R., Cunningham, G. F., Wensnahan, M., Rigor, I., Zwally, H. J., and Yi, D.: Thinning and volume loss of the Arctic Ocean sea ice cover: 2003-2008, J. Geophys. Res., 114, C07005, doi:10.1029/2009JC005312, 2009.

Lindsay, R. and Schweiger, A.: Arctic sea ice thickness loss determined using subsurface, aircraft, and satellite observations, The Cryosphere, 9, 269-283, doi:10.5194/tc-9-269-2015, 2015.

Lindsay, R. and Zhang, J.: Assimilation of ice concentration in an ice-ocean model, J. Atmos. Oceanic Tech., 23, 742-749, 2006.

Mori, M., Watanabe, M., Shiogama, H., Inoue, J., and Kimoto, M.: Robust Arctic sea-ice influence on the frequent Eurasian cold winters in past decades, Nat. Geosci., 7, 869-873, doi:10.1038/NGEO2277, 2014.

Msadek, R., Vecchi, G. A., Winton, M., and Gudgel, R. G.: Importance of initial conditions in seasonal predictions of Arctic sea ice extent, Geophys. Res. Lett., 41, 5208-5215, doi:10.1002/2014GL060799, 2014.

Nakanowatari, T., Sato, K., and Inoue, J.: Predictability of the Barents sea ice in early winter: Remote effects of oceanic and atmospheric thermal conditions from the North Atlantic, J. Clim., 27, 8884-8901, doi:10.1175/JCLI-D-14-00125.1, 2014.

Peterson, K. A., Arribas, A., Hewitt, H. T., Keen, A. B., Lea, D. J., and McLaren, A. J.: Assessing the forecast skill of Arctic sea ice extent in the GloSea4 seasonal prediction system, Clim Dyn., 44, 147-162, doi:10.1007/s00382-014-2190-9, 2015.

Pithan, F., and Mauritsen, T.: Arctic amplification dominated by temperature feedbacks in contemporary climate models, Nat. Geosci., 7, 181-184, doi:10.1038/NGEO2071, 2014.

Polyakov, I. V., Walsh, J. E., and Kwok, R.: Recent changes of arctic multiyear sea ice coverage and the likely causes, Bull. Amer. Meteor. Soc., 93, 145-151, doi:10.1175/BAMS-D-11-00070.1, 2012.

Sigmond, M., Fyfe, J. C., Flato, G. M., Kharin, V. V., and Merryfield, W. J.: Seasonal forecast skill of Arctic sea ice area in a dynamical forecast system, Geophys. Res. Lett., 40, 529-534, doi:10.1002/grl.50129, 2013.

Sigmond, M., Reader, M. C., Flato, G. M., Merryfield, W. J., and Tivy, A.: Skillful seasonal forecast of Arctic sea ice retreat
5   and advance dates in a dynamical forecast system, Geophys. Res. Lett., 43, 12457-12465, doi:10.1002/2016GL071396, 2016.

Smedsrud, L. H., Esau, I., Ingvaldsen, R. B., Eldevik, T., Haugan, P. M., Li, C., Lien, V. S., Olsen, A., Omar, A. M., Otterå, O. H., Risebrobakken, B., Sandø, A. B., Semenov, V. A., and Sorokina, S. A.: The role of the Barents Sea in the Arctic climate system, Rev. Geophys., 51, 415-449, doi:10.1002/rog.20017, 2013.
10

Stark, J. D., Ridley, J., Martin, M., and Hines, A.: Sea ice concentration and motion assimilation in a sea ice-ocean model, J. Geophys. Res., 113, C05S91, doi:10.1029/2007JC004224, 2008.

Stephenson, S. R., Brigham, L. W., and Smith, L. C.: Marine accessibility along Russia's Northern Sea Route, Polar Geogr.,
15   37(2), 111-133, http://dx.doi.org/10.1080/1088937X.2013.845859, 2014.

Stocker, T. F., Qin, D., Plattner, G. K., Tignor, M., Allen, S. K., Boschung, J., Nauels, A., Xia, Y., Bex, V., and Midgley, P. M.: IPCC, 2013: Climate Change 2013: The Physical Science Basis. Contribution of Working Group I to the Fifth Assessment Report of the Intergovernmental Panel on Climate Change, Cambridge University Press, Cambridge, United
20   Kingdom and New York, NY, USA, 1535 pp, doi:10.1017/CBO9781107415324, 2013.

Stroeve, J. C., Crawford, A. D., and Stammerjohn, S.: Using timing of ice retreat to predict timing of fall freeze-up in the Arctic, Geophys. Res. Lett., 43, 6332-6340, doi:10.1002/2016GL069314, 2016.

25   Tatebe, H., Ishii, M., Mochizuki, T., Chikamoto, Y., Sakamoto, T. T., Komuro, Y., Mori, M., Yasunaka, S., Watanabe, M., Ogochi, K., Suzuki, T., Nishimura, T., and Kimoto, M.: The initialization of the MIROC climate models with hydographic data assimilation for decadal prediction, J. Meteorol. Soc. Jpn., 90A, 275-294, doi:10.2151/jmsj.2012-A14, 2012.

Tietsche, S., Day, J. J., Guemas, V., Hurlin, W. J., Keeley, S. P. E., Matei, D., Msadek, R., Collins, M., and Hawkins, E.:
30   Seasonal to interannual Arctic sea ice predictability in current global climate models, Geophys. Res. Lett., 41, 1035-1043, doi:10.1002/2013GL058755, 2014.

Wang, L., Yuan, X., Ting, M., and Li, C.: Predicting summer Arctic sea ice concentration intraseasonal variability using a vector autoregressive model, J. Clim., 29(4), 1529-1543, doi:10.1175/JCLI-D-15-0313.1, 2016.

Wang, W., Chen, M., and Kumar, A.: Seasonal prediction of Arctic sea ice extent from a coupled dynamical forecast system, Mon. Weather Rev., 141, 1375-1394, doi:10.1175/MWR-D-12-00057.1, 2013.

5   Watanabe, M., Suzuki, T., O'ishi, R., Komuro, Y., Watanabe, S., Emori, S., Takemura, T., Chikira, M., Ogura, T., Sekiguchi, M., Takata, K., Yamazaki, D., Yokohata, T., Nozawa, T., Hasumi, H., Tatebe, H., and Kimoto, M.: Improved climate simulation by MIROC5: Mean states, variability, and climate sensitivity, J. Clim., 23, 6312–6335, doi:10.1175/2010JCLI3679.1, 2010.

10

15

20

25

30

Figure captions

Figure 1: Lagged auto-correlation coefficients of the detrended SIE_{AO} anomaly derived from (a) observations (Ishii et al. (2006) and Ishii and Kimoto (2009)) and (b) a model control simulation, for each start month, against lead time, following

5   Day et al. (2014b). Solid and dashed lines denote values for the September and March target months, respectively. Black dots indicate statistical significance at the 95 % confidence level based on a two-sided Student's t-test with 30 and 200 degrees of freedom in observation and model, respectively.

Figure 2: Lead-time dependence of (a) SIE_{AO} ACC and (b) SIE_{AO} RMSE ($\times 10^6$ km^2) for hindcasts started in January, April,

10   July, and October. SIE_{AO} ACC (RMSE) scores of hindcasts that are higher (lower) than those of the persistence forecast and statistically significant at the 95 % confidence level based on a two-sided Student's t-test are denoted by black dots. Time series of the detrended SIE_{AO} anomaly for (c) September and (d) December, from the observation (black line), assimilation (red line), and hindcasts started from July 1st and January 1st (blue line). Blue shading indicates the ensemble spread. In (c), September SIE_{AO} started from April 1st is superimposed by aqua line and shading.

15

Figure 3: Lagged correlation coefficients between the detrended SIE_{AO} anomaly and (a–c) the detrended SIV_{AO} anomaly and (d–f) the detrended OHC_{AO} anomaly. Left, middle, and right panels indicate values obtained from the control run (CTRL), the hindcasts started from January 1st (HIND.JAN), and the hindcasts started from July 1st (HIND.JUL), respectively. Black dots indicate statistical significance at the 95 % confidence level based on a two-sided Student's t-test with 30 and 200

20   degrees of freedom in the observation and model. Note that the horizontal and vertical axes in the hindcasts started from July 1st are different from those in the control run and the hindcasts started from January 1st.

Figure 4: Lagged correlation (colors) and regression (contours) coefficients between the SIE_{AO} anomaly ($\times 10^6$ km^2) in December and (a) SIC anomaly (%) at a lag of 0 months, (b) SIT anomaly (cm) at a lag of 0 months, and OHC anomalies

25   ($\times 10^{18}$ J) at lags of (c) -9, (d) -6, (e) -3, and (f) 0 months, in regions from 60° to 90° N on the basis of the hindcasts started from January 1st. Contours are drawn at intervals of 5 (%) from 5 to 25 for SIC and 10 (cm) from 10 to 40 for SIT. In (c–f), the contours are drawn from -1.0 to -0.1 ($\times 10^{18}$ J) at intervals of 0.1 ($\times 10^{18}$ J). Stippling indicates regions with statistically significant correlation coefficients at the 95 % confidence level. White shading indicates areas where the bottom of the MLD is below a depth of 200 m or sea ice does not exist. A latitude circle of 65° N is also indicated by a thin solid line.
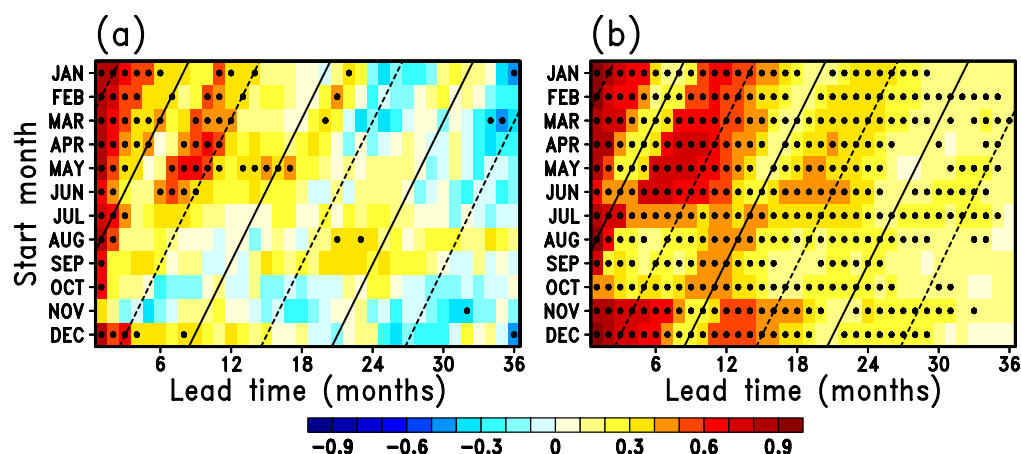
30

Figure 1. Lagged auto-correlation coefficients of the detrended SIE$_{AO}$ anomaly derived from (a) observations (Ishii et al. (2006) and Ishii and Kimoto (2009)) and (b) a model control simulation, for each start month, against lead time, following Day et al. (2014b). Solid and dashed lines denote values for September and March target months, respectively. Black dots indicate statistical significance at the 95% confidence level based on a two-sided Student's t-test with 30 and 200 degrees of freedom in observation and model, respectively.
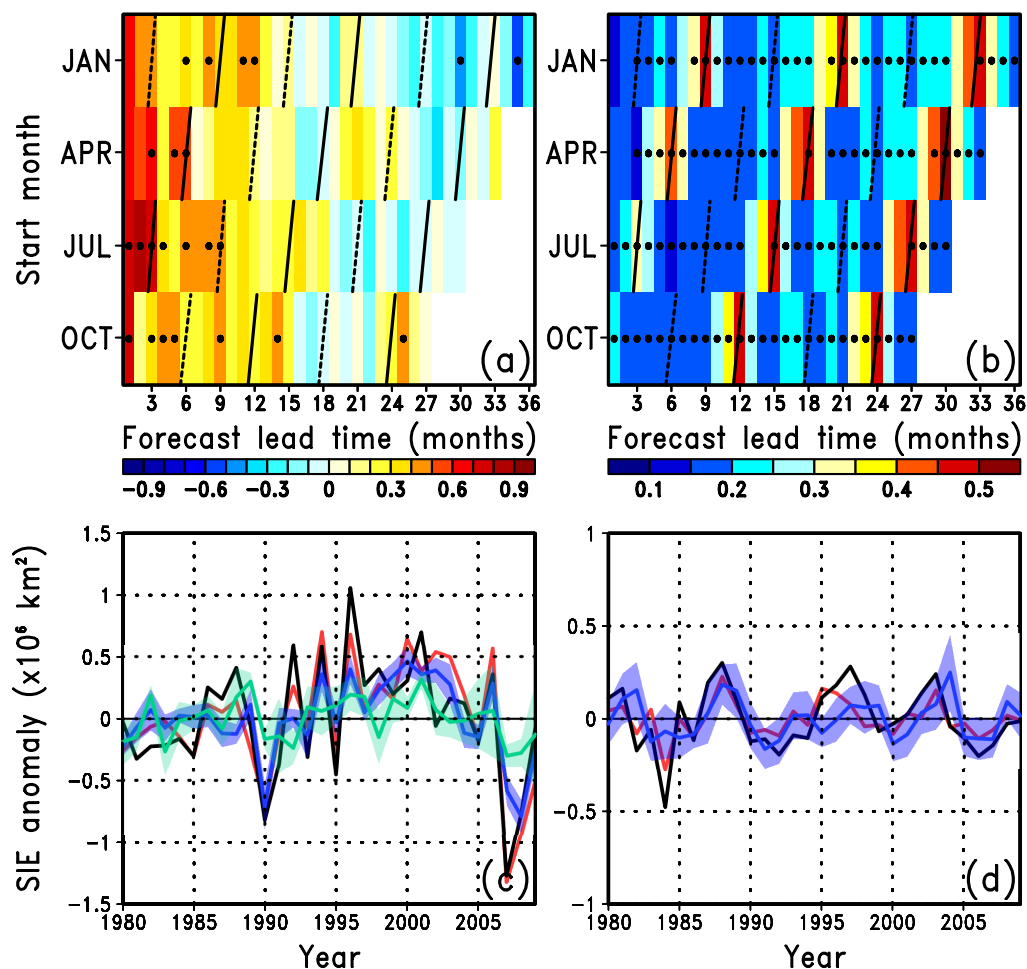
5

10

15

20

13

Figure 2. Lead-time dependence of (a) SIE_{AO} ACC and (b) SIE_{AO} RMSE ($\times 10^6$ km^2) for January, April, July, and October start hindcasts. SIE_{AO} ACC (RMSE) scores of hindcasts, which are higher (lower) than those of persistence forecast and statistical significance at the 95% confidence level based on a two-sided Student's t-test, are denoted by black dots. Time series of the detrended SIE_{AO} anomaly for (c) September and (d) December, from the observation (black line), assimilation (red line), and hindcasts started from July 1st and January 1st (blue line). Blue shading indicates the ensemble spread. In (c), September SIE_{AO} started from April 1st is superimposed by aqua line and shading.
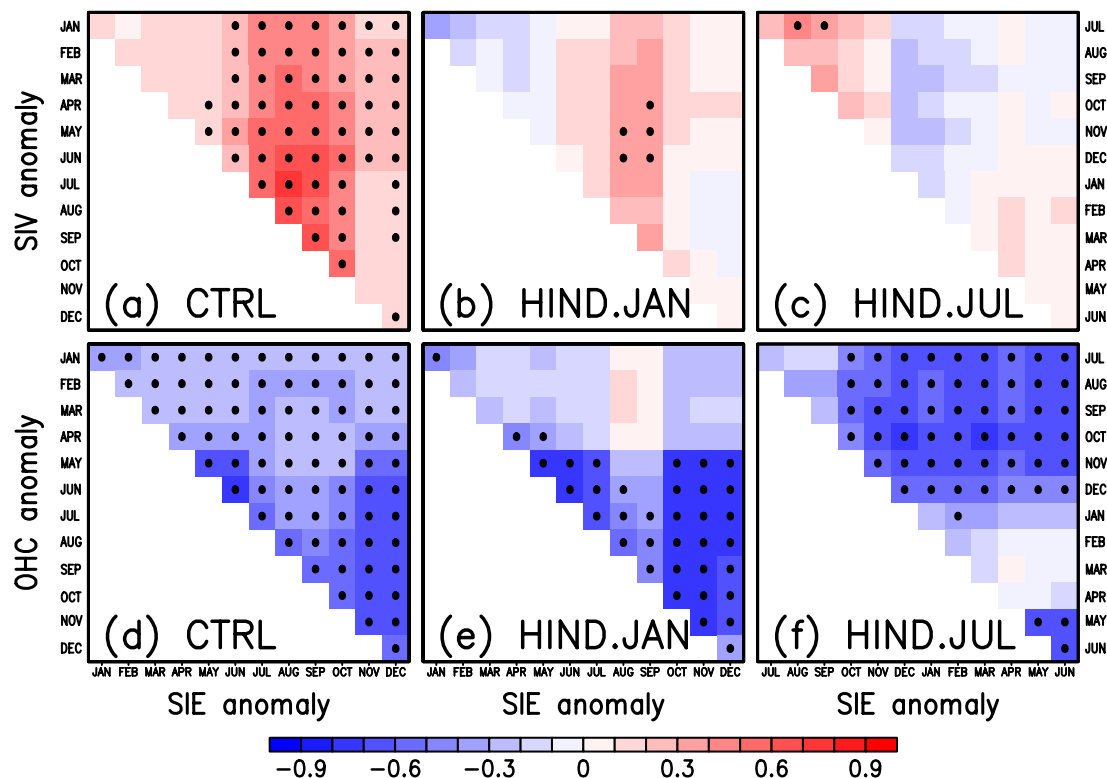
14

Figure 3. Lagged correlation coefficients between the detrended SIE$_{AO}$ anomaly and (a–c) the detrended SIV$_{AO}$ anomaly and (d–f) the detrended OHC$_{AO}$ anomaly. Left, middle, and right panels indicate values obtained from the control run (CTRL), the hindcasts started from January 1st (HIND.JAN), and the hindcasts started from July 1st (HIND.JUL), respectively. Black dots indicate statistical significance at the 95% confidence level based on a two-sided Student's t-test with 30 and 200 degrees of freedom in observation and model. Note that horizontal and vertical axes in the hindcasts started from July 1st are different from those in the control run and the hindcasts started from January 1st.
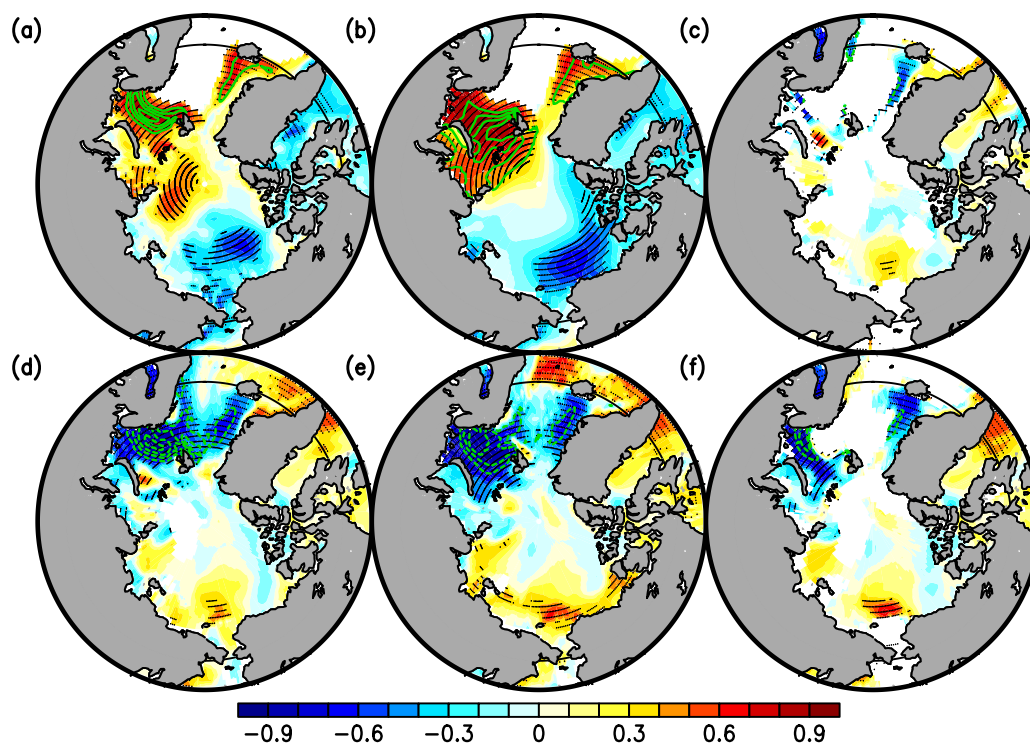
15

Figure 4. Lagged correlation (colors) and regression (contours) coefficients between SIE_{AO} anomaly ($\times10^6$ km^2) in December and (a) SIC anomaly (%) at lag 0 month, (b) SIT anomaly (cm) at lag 0 month, and OHC anomalies ($\times10^{18}$ J) at lag (c) -9, (d) -6, (e) -3, and (f) 0 months, in regions from 60° to 90°N on the basis of the hindcasts started from January 1st. Contour intervals are 5 (%) from 5 to 25 for SIC and 10 (cm) from 10 to 40 for SIT. In (c–f), contours are drawn from -1.0 to -0.1 ($\times10^{18}$ J) with interval of 0.1 ($\times10^{18}$ J). Stipples indicate regions with statistically significant correlation coefficient at the 95% confidence level. White shading indicates areas where the bottom of the MLD is below a depth of 200 m or sea ice does not exist. Latitude circle of 65°N is also indicated by thin solid line.